Near Surface Geophysics, 2014, **12**, 505-514 doi:10.3997/1873-0604.2014005

Global inversion of GPR traveltimes to assess uncertainties in CMP velocity models

Göran Hamann* and Jens Tronicke

Institut für Erd- und Umweltwissenschaften, Universität Potsdam, Karl-Liebknecht Straße 24, 14476 Potsdam, Germany

Received June 2013, revision accepted November 2013

ABSTRACT

Velocity models are essential to process two- and three-dimensional ground-penetrating radar (GPR) data. Furthermore, velocity information aids the interpretation of such data sets because velocity variations reflect important material properties such as water content. In many GPR applications, common midpoint (CMP) surveys are routinely collected to determine one-dimensional velocity models at selected locations. To analyse CMP data gathers, spectral velocity analyses relying on the normal-moveout (NMO) model are commonly employed. Using Dix's formula, the derived NMO velocities can be further converted to interval velocities which are needed for processing and interpretation. Because of the inherent assumptions and limitations of such approaches, we investigate and propose an alternative procedure based on the global inversion of reflection traveltimes. We use a finite-difference solver of the Eikonal equation to accurately solve the forward problem in combination with particle swarm optimization (PSO) to find one-dimensional GPR velocity models explaining our data. Because PSO is a robust and efficient global optimization tool, our inversion approach includes generating an ensemble of representative solutions that allows us to analyse uncertainties in the model space. Using synthetic data examples, we test and evaluate our inversion approach to analyse CMP data collected across typical near-surface environments. Application to a field data set recorded at a well-constrained test site including a comparison to independent borehole and direct-push data, further illustrates the potential of the proposed approach, which includes a straightforward and understandable appraisal of non-uniqueness and uncertainty issues, respectively. We conclude that our methodology is a feasible and powerful tool to analyse GPR CMP data and allows practitioners and researchers to evaluate the reliability of CMP derived velocity models.

INTRODUCTION

In many archaeological, engineering, environmental, and geological applications, ground-penetration radar (GPR) is an important geophysical tool to investigate near-surface environments (e.g., Davis and Annan 1989; Jol 2008). To accurately image subsurface structures such as geological layering or man-made objects with GPR, information regarding GPR velocity and its variations is crucial (Tillard and Dubois 1995). For example, migration routines require an accurate velocity model to move dipping reflections to their correct position, unravel crossing events, and collapse diffractions (Yilmaz 2001). Further processing steps whose success is closely related to the accuracy of the available velocity information include time-to-depth conversions and elevation corrections (Annan 2005; Cassidy 2009). In addition, GPR velocity is increasingly used to aid the interpretation of reflection images and to quantitatively characterize the subsurface; i.e., to estimate petrophysical properties such as water content or porosity (e.g., Greaves *et al*. 1996; van Overmeeren *et al*. 1997; Huisman *et al*. 2003; Tronicke *et al*. 2004; Steelman and Endres 2012; Hamann *et al*. 2013).

To determine a GPR velocity model, different surveying approaches can be employed. Cross-hole tomography (e.g., Binley *et al*. 2001; Tronicke *et al*. 2002) and vertical radar profiling (e.g., Cassiani *et al*. 2004; Tronicke and Knoll 2005) can provide detailed information regarding subsurface velocity variations. However, the feasibility of such borehole-based techniques is often limited due the limited number of available boreholes. Thus, the most common surveying strategies to obtain velocity information rely on surface-based common-offset (CO) or multi-offset survey geometries. When using CO data, hyperbola-shaped diffraction events, associated with isolated objects or sharp discontinuities, can be analysed because the geometry of these events depends on the subsurface velocity distribution (e.g., Moore *et al*. 1999; Bradford and Harper 2005; Porsani and Sauck 2007). However, when the number and/or distribution of diffraction events is limited, the results of such analyses may not provide sufficient detail

* hamann@geo.uni-potsdam.de

regarding velocity variations. Thus, a limited number of multi-offset CMP gathers is typically recorded to obtain one-dimensional (1D) velocity models at selected locations in the surveyed area (Annan 2005). The analysis of such CMP data is commonly performed using reflection seismic processing tools based on the normal-moveout (NMO) model (e.g., spectral velocity analysis; Yilmaz 2001). Here, we have to consider the fundamental assumptions of such NMO based velocity analysis, which include small offset-to-depth ratios, small velocity gradients, and plane horizontal reflectors (Al-Chalabi 1973, 1974). Considering these assumptions, various studies have investigated the influence of different sources of errors on the derived GPR velocity estimates (Tillard and Dubois 1995; Jacob and Hermance 2004; Becht *et al*. 2006; Booth *et al*. 2010, 2011) also considering the relevant seismic literature (e.g., Taner and Köhler 1969; Levin 1971; Hajnal and Sereda 1981; Alkhalifah 1997). For example, Booth *et al*. (2010) investigated timing errors associated with the finite duration of the GPR wavelet and their influence on the derived velocity model while Becht *et al*. (2006) studied the influence of layer dip and velocity contrast (spatial velocity changes that causes reflection and refraction). Summarizing the findings of the above cited publications illustrates that GPR interval velocity models derived from NMO based analyses may show significant errors hindering a detailed interpretation of the derived velocity variations (e.g., in terms of different petrophysical parameters). As an alternative, Harper and Bradford (2003) used the least-squares inversion approach of Zelt and Smith (1992) to reconstruct a 1D velocity model from manually picked reflection traveltimes. Although the assumptions inherent in NMO based velocity analyses are avoided by this approach, we have to consider the limitations of applying such a linearized inversion strategy to the non-linear problem of reflected traveltime inversion (e.g., Sen and Stoffa 1995). For example, when using local optimization approaches the influence of the starting model has to be considered because the final solution obtained by such an approach may critically depend on the initial model (Menke 1989; Aster *et al*. 2013).

There is also a growing interest in multi-offset GPR surveying strategies adapting multi-fold acquisition geometries known from reflection seismics. The resulting data sets allow for the generation of densely-sampled 2D or even 3D velocity models using techniques adapted from seismic data processing (Greaves *et al*. 1996; Cai and McMechan 1999; Pipan *et al*. 1999; Becht *et al*. 2006; Bradford *et al*. 2009). In addition to NMO based workflows, this also includes the application of techniques known from seismic prestack migration velocity analysis which, for example, also allow for considering dipping reflectors and lateral velocity variations (Leparoux *et a*l. 2001; Bradford 2006). Although the advantages of multi-fold data acquisition and analysis are well documented (see references above), the increased field and processing effort is often considered as a major limitation (e.g., Booth *et al*. 2008) and, thus, also today the analysis of individual CMP gathers is crucial for extracting velocity information from surface-based GPR data.

In this study, we propose a novel workflow to analyse GPR CMP data. Our methodology is based on inverting reflection traveltimes using a global optimization approach known as particle swarm optimization (PSO). Combined with an accurate forward modelling procedure based on a fast marching eikonal solver (Sethian 1996; Fomel 1997; Sethian and Popovici 1999), our methodology avoids the fundamental assumptions of NMO based analyses and allows us to directly invert for interval velocity models. We also generate representative ensembles of acceptable solutions which allows us to appraise uncertainties in the model space and, thus, evaluate the reliability of CMP velocity models. In the following, we start by reviewing NMO based spectral velocity analysis. After that, we introduce the fundamentals of our PSO based inversion scheme which, then, is tested and evaluated using synthetic data examples. Finally, we apply our method to GPR field data recorded across sand and gravel dominated deposits. Comparing the resulting velocity models to velocity models derived from NMO based analysis and to independent direct-push and borehole data, respectively, allows us to evaluate our results including the derived uncertainty estimates.

SPECTRAL VELOCITY ANALYSIS

One of the standard tools for analysing individual CMP gathers is spectral velocity analysis (Taner and Köhler 1969; Yilmaz 2001; Annan 2005). Assuming a layered subsurface consisting of isotropic and homogeneous layers separated by plane interfaces, NMO based analyses are used to test a set of user-specified velocity values. The velocity spectrum is generated using a predefined measure of coherency (such as semblance or unnormalized cross-correlation) across the data gather in a predefined time window centred on hyperbolic trajectories calculated by

$$t_{NMO}(x) = \sqrt{t_0^2 + \frac{x^2}{v_{NMO}^2}}, \quad (1)$$

where x is the transmitter-receiver offset, t_0 the zero-offset traveltime, and v_{NMO} the normal-moveout velocity. The optimum stacking velocities are then selected by analysing the maxima in the resulting velocity spectrum (i.e., calculated coherency values as a function of tested velocities and traveltimes) corresponding to primary reflection events in the analysed CMP gather. Assuming horizontal interfaces and small transmitter-receiver offsets (compared to the reflector depth), the derived stacking velocities can be approximated by root-mean square (RMS) velocities which, then, can be converted to interval velocities using the classical equation developed by Dix (1955).

To illustrate the traveltime errors associated with equation 1, we present a modelling example employing typical GPR offset ranges and velocity distributions (i.e., decreasing velocity with increasing depth). We compare t_{NMO} (equation 1) with traveltimes computed using a fast marching eikonal solver (t_{mod}), which is known as an accurate, stable, and computational efficient method for traveltime modelling (Sethian 1996; Fomel 1997; Sethian and

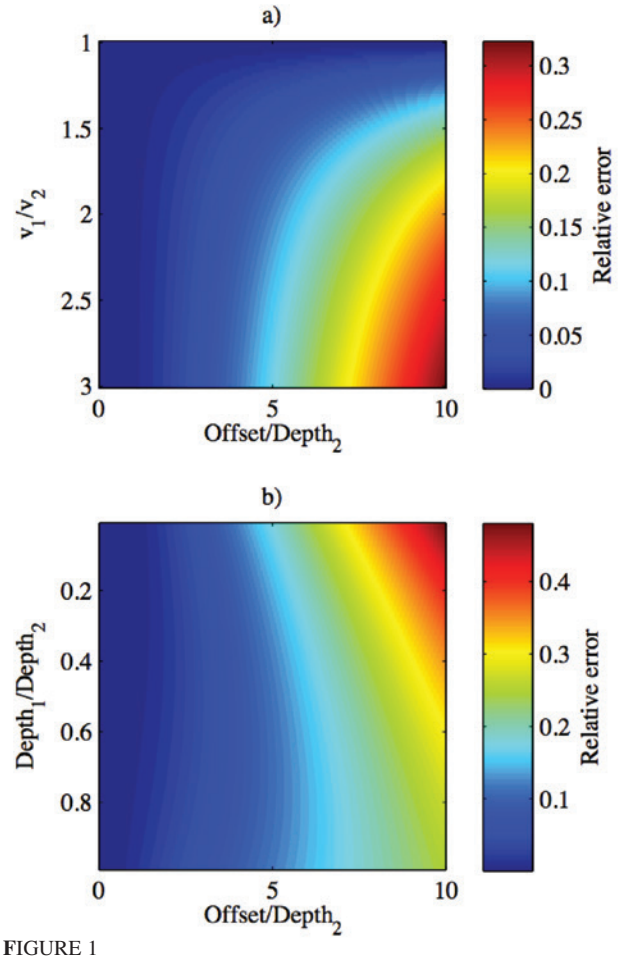

FIGURE 1

Relative errors associated with the NMO model (equation 1) for horizontally layered velocity models consisting of two interfaces (at depths Dpeth$_1$ and Depth$_2$) defining two homogenous layers with velocities v_1 and v_2. (a) Relative errors as a function of the offset-to-depth ratio and the velocity ratio between the upper and the lower layer for a fixed ratio of one between the thickness of the first and the second layer. (b) Relative errors as a function of the offset-to-depth ratio and the depth ratio between the upper and the lower layer for a fixed velocity ratio of $v_1/v_2 = 3$. For details see text.

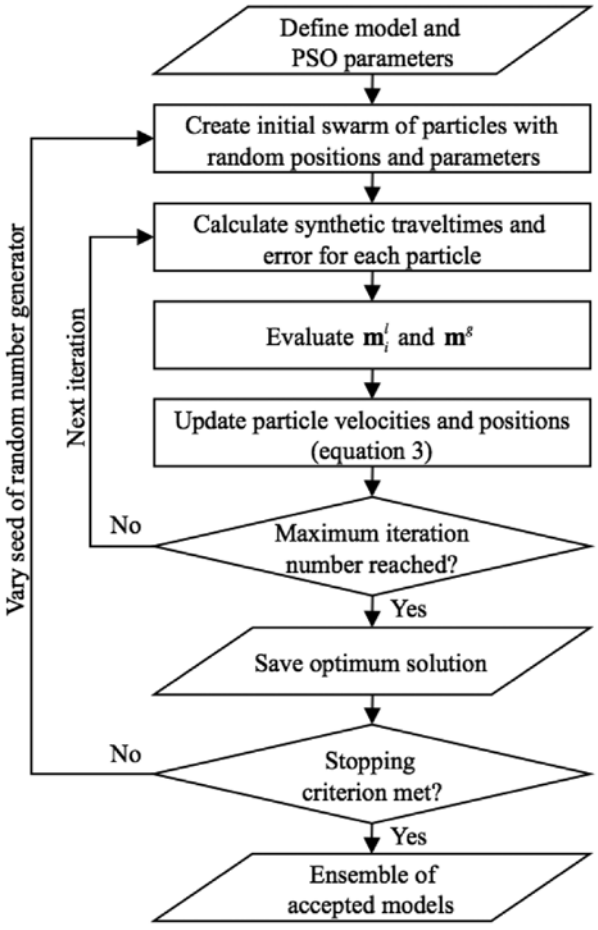

FIGURE 2

Flow diagram illustrating the key proposed PSO-based global inversion procedure of CMP reflection traveltimes. For details see text.

Popovici 1999). For horizontally layered velocity models consisting of two interfaces, we compare the traveltime differences for the deeper reflector using relative errors calculated as $(t_{NMO} - t_{mod}) / t_{NMO}$. In Fig. 1a, we show the resulting errors as a function of the offset-to-depth ratio (considering the depth of lowermost layer noted by Depth$_2$) and the velocity ratio between the upper and the lower layer (v_1/v_2). Here, the ratio between the thickness of the first and the second layer is fixed to one. The errors increase for increasing velocity contrasts and increasing offset-to-depth ratios and can be easily in the order of 5 % to 10 % and more. In Fig. 1b, we illustrate the relative errors as a function of the offset-to-depth ratio and the depth ratio between the upper and the lower layer (Depth$_1$/Depth$_2$) while the velocity ratio is fixed to $v_1/v_2 = 3$. Again, errors increase with increasing offset-to-depth ratios while the influence of the depth ratio between the two interfaces is more pronounced for larger values of the offset-to-depth ratio. For this case, in a) the first layer has a thickness of half a metre and one velocity has to be fixed and the other varied. In b) we proceed respectively for the layer thicknesses and we set the velocities to constant.

The presented modelling exercise demonstrates the limitations of the NMO model for rather typical GPR situations and indicates that the procedure of deriving 1D velocity models from individual GPR CMP gathers using NMO based analyses is prone to errors. Especially, if we are interested in an interval velocity model, for example, to aid GPR data interpretation, we should employ techniques avoiding the assumptions inherent in NMO based approaches. Furthermore, an appropriate velocity analysis tool should allow us to appraise resolution and non-uniqueness issues, and thus quantify the uncertainties expected for a CMP based velocity model. With this motivation, we now introduce our methodology based on the global inversion of reflection traveltimes.

GLOBAL INVERSION OF CMP TRAVELTIMES

In this section, we describe the methodological basics of our global inversion approach which is outlined in Fig. 2. We introduce the employed global optimization method which is known as particle swarm optimization (PSO) including the necessary details of our implementation to invert GPR traveltime data observed in CMP data sets.

Inspired by the social behavior of birds and fishes, PSO has been introduced by Kennedy and Eberhard (1995) as a tool to globally solve optimization problems. Due to its flexibility and computational efficiency the method has been recognized as a feasible tool in a variety of applications (Poli 2008). PSO based inversion method is rigorous in terms of implementation and shows faster convergence compared to other global optimization approaches (e.g., simulated annealing approaches). We will show that the PSO method is an elegant, fast and promising way to describe GPR CMP traveltime data, made plausible with more precise and complete initial state independent optimized, statistically representative subsurface velocity models with uncertainties, and which enables further quantitative soil parameter predictions. More recently, there is a growing interest in using PSO to solve typical inverse geophysical problems (Shaw and Srivastava 2007; Fernández Martínez *et al*. 2010; Monteiro Santos 2010; Tronicke *et al*. 2012; Wilken and Rabbel 2012). Here, we use PSO to globally invert traveltimes determined from GPR CMP surveys and our implementation basically follows Tronicke *et al*. (2012) who employed PSO to invert crosshole seismic traveltime data. A standard personal machine with quart core and 6 GB RAM was used to achieve results such as those demonstrated in this paper.

In PSO, the swarm consists of a number of particles which explore a predefined model space. The location of the *i*-th particle in the model space is represented by a model vector $\mathbf{m_i}$. Here, we invert for a 1D velocity model parameterized using a predefined number of layers and, thus, $\mathbf{m_i}$ is defined by layer (interval) velocities and layer thicknesses. The fitness of a particle at its current location in the model space is evaluated using an objective function L_i which we define as

$$L_i = \frac{1}{N}\sum_{j=1}^{N}\sqrt{\left(t_{obs,j} - t_{mod,j}\right)^2}\,, \tag{2}$$

where t_{obs} and t_{mod} are observed and forward modelled traveltimes of primary reflections, respectively, and N represents the total number of traveltimes used for the inversion. We calculate t_{mod} using a fast marching eikonal solver because this technique is accurate (e.g., accounts for refraction across layer boundaries) and computationally efficient (Sethian 1996; Fomel 1997; Sethian and Popovici 1999).

In PSO, to ensure information exchange within the swarm, the movement of an individual particle through the model space is determined by combining the history of its own fitness (cognitive component) with those of the entire swarm (social component). Combining these components with some random perturbations results in a vector Φ (known as the velocity vector in PSO terminology) that controls the movement of the particles during the iterative optimization procedure. At iteration k+1, the new location of the i-th particle is calculated by

$$\begin{aligned}\Phi_i^{k+1} &= w\Phi_i^k + c_1 r_1^{k+1}\left(m_i^l - m_i^k\right) + c_2 r_2^{k+1}\left(m^g - m_i^k\right),\\ m_i^{k+1} &= m_i^k + \Phi_i^{k+1},\end{aligned} \tag{3}$$

where m_i^l is the personal best position of the i-th particle, m^g is the global best position of the entire swarm, r_1 and r_2 are randomly drawn from a uniform distribution in [0,1], w is the inertia weight serving as a memory of previous velocities, and c_1 and c_2 are the acceleration constants controlling the relative proportion of cognition and social interaction within the swarm. After van den Bergh (2002) convergence is ensured if w, c_1, and c_2 are selected in such a way that they satisfy $(c_1 + c_2)/2 - 1 < 1$.We set $w = 0.7298$ and $c_1 = c_2 = 1.4962$, which fulfills the given relation and has proven to provide efficient convergence in numerous different optimization problems (Eberhart and Shi 2000; and Clerk and Kennedy 2002).

When starting the PSO optimization procedure, Φ is set to zero and the particles are randomly initialized in the predefined model space. Constraining the model space (i.e., possible values for layer velocities and thicknesses) to physically and geologically reasonable parameter values, and also considering available a priori information, helps to speed up the convergence behaviour of the algorithm. After this initialization, the forward problem is solved for each particle, the objective function (equation 2) is evaluated, and m_i^l and m^g are stored. In the following iterations, the model vectors are updated (equation 3) and compared to m_i^l and m^g. If the new model of the i-th particle is better than the current personal best model and the best global model, m_i^l and m^g are updated. This procedure is repeated until a predefined stopping criterion is reached (inner loop in Fig. 2). The final m^g represents the optimum solution; i.e., a 1D velocity model explaining our traveltime data set.

Before starting the PSO optimization procedure, we have to define the number of particles and the stopping criteria (maximum number of iterations and/or acceptable value of the objective function). To find optimum parameters in terms of desired error level as well as computational effort for a specific problem, some initial parameter testing is required. For the CMP examples presented in this study, generally 20 particles and 300 iterations are sufficient to explain our data. Furthermore, our parameter tests have shown that further increasing the PSO parameters number of particles and number of iterations has no critical impact on the obtained results, but on computation time. In addition, we also have to specify the number of layers in our model parameterization. Here, also considering the results of NMO-based velocity analyses we have to interpret our CMP data in terms of primary reflection events, and multiple reflections have to be identified and excluded from the analysis.

GENERATING A REPRESENTATIVE ENSEMBLE

As indicated by the outer loop in Fig. 2, we repeat the above described PSO optimization procedure with different randomly generated starting models and different seeds of the random number generator. Herewith, we generate an ensemble of models explaining the data equally well (Fernández Martínez *et al*. 2010; Tronicke *et al*. 2012). Analysing such an ensemble allows us to assess uncertainty and nonuniqueness issues in the formulated inverse problem; for example, to appraise how well a layer boundary or the velocity of a certain layer is resolved. To evaluate the representativeness of the generated ensemble, we follow Sen and Stoffa (1995) and compute the elements M_{ij} of the posterior correlation matrix **M** by

$$M_{ij} = \frac{C_{ij}}{\sqrt{C_{ii}C_{jj}}}, \tag{4}$$

where C_{ij} is an element of the posterior covariance matrix **C**. The matrix **C** is calculated from the ensemble of accepted solutions m^g by

$$C = \frac{1}{M}\sum_{j=1}^{M}\left(m_j^g - \left\langle m^g \right\rangle\right)\left(m_j^g - \left\langle m^g \right\rangle\right)^T, \tag{5}$$

where M is number of models within the ensemble and

$$\left\langle m^g \right\rangle = \frac{1}{M}\sum_{j=1}^{M} m_j^g . \tag{6}$$

By analysing changes in **M** during the inversion procedure (i.e., ensemble generation), we can evaluate the representativeness of the ensemble (Sen and Stoffa 1995). If no significant variations in **M** are detected when new models are added to the ensemble, we assume that the ensemble is representative and allows for reliable posterior statistical analyses. For our inversion problem, we found that an ensemble consisting of 100 models characterized by an acceptable data fit can typically be regarded as representative. Because the found empirical distributions of the model parameters are typically not following a normal distribution, we use robust statistical measures to analyse the distributions in more detail. For our synthetic and field examples, we compute the median, the 5th to 95th percentile, and the 25th to 75th percentile to characterize the central tendency and the spread of the underlying parameter distributions. In addition, the matrix **M** (equation 4) can be used to analyse correlations between the individual model parameters, providing further insights into the formulated inverse problem and employed model parameterization, respectively.

SYNTHETIC EXAMPLES

In this section, we test and evaluate the proposed workflow using synthetic examples. We generate synthetic traveltime data sets simulating traveltimes from reflected events as observed in GPR CMP surveys, and invert these data using our PSO based inversion procedure. Furthermore, such synthetic examples allow us to analyse ensemble characteristics and the uncertainties that can be expected for typical CMP data sets recorded across typical subsurface environments.

Example 1

The first synthetic example represents a CMP survey recorded with a trace spacing of 0.1 m and maximum offset of 15 m across a ten-layer case where each layer is characterized by a constant interval velocity of 100 m/μs and a thickness of 1 m (i.e., the deepest layer boundary is found at 10 m depth). With this model we want to investigate depth dependent model characteristics, which might be related to decreasing moveout with increasing interface depth for a fixed CMP geometry. The results of globally inverting the corresponding noise-free traveltime data set are presented in Fig. 2. For this case thicknesses vary between 0.5 to 1.5 m and velocities vary between 0.08 to 0.12 m/ns, as PSO search space limits. We show the median, the 25th to 75th, and the 5th to 95th percentile calculated from the ensemble of model parameter distributions (interval velocity and thickness of layers number one to ten where layer number one corresponds to the uppermost layer) and compare it to the corresponding input values. The input values of velocity and thickness are well recovered by the median values of the parameter distributions (maximum discrepancies <2%). In Fig. 3a, the 25th to 75th and the 5th to 95th percentile values indicate maximum uncertainties of ~7% and ~15%, respectively, with a trend of increasing uncertainty with increasing depth (i.e., increasing layer number). For the thicknesses (Fig. 3b), we observe no characteristic trend with depth and the 25th to 75th and the 5th to 95th percentile values indicate uncertainties of ~5–8% and ~13–22%, respectively. The observation of increasing uncertainties in velocity with increasing depth can be related to the lower moveout observed for the deeper reflection events in comparison to shallow reflections at the same offset; i.e., shallow events are more sensitive to a certain variation in velocity than deeper events.

In Fig. 4, we show the posterior correlation matrix calculated from the final ensemble of accepted solutions. This matrix can be used to analyse the interdependence between different model parameters. In Fig. 4, model parameters one to ten correspond to the layer thicknesses of layer number one to ten while parameters eleven to twenty represent the corresponding layer velocities. We observe high positive correlations between the thickness and the velocity of a specific layer while high negative correlations are observed between thickness and velocity of a specific layer and the thicknesses and velocities of the neighbouring layers. These observations illustrate that the uncertainties associated with the corresponding pairs of model parameters are highly correlated and anticorrelated, respectively, and that the corresponding parameters can not be independently resolved by the data set; i.e., only some linear combination of the parameters are resolved (Tarantola 2005). For example, due to the high positive correlations (close to one) between layer thickness and velocity we can not expect to accurately resolve both parameters for a specific layer; i.e., if one of the parameters is estimated too high

or too low this can be easily compensated by increasing or decreasing the other corresponding parameter (e.g., layer five in Fig. 3). Thus, there is an inherent non-uniqueness in the formulated inverse problem which we have to be aware of when analysing the inversion results. Our experience with a number of different synthetic and field CMP data sets shows that we always observe similar patterns and correlations in the resulting posterior correlation matrices and, thus, these matrices will not be shown for the following examples.

Example 2

Our second synthetic example simulates a rather typical hydrogeological situation where a shallow groundwater table results in a sharp velocity decrease. In such situations, we might be interested in resolving rather small velocity variations in the water saturated zone which, for example, could be interpreted in terms of porosity variations. Therefore, the input five-layer velocity model comprises a 2 m thick top layer with a velocity of 100 m/μs followed by a sequence of four 2 m thick layers characterized by velocities of 50 m/μs and 60 m/μs, respectively. The CMP survey geometry is identical to the first example; i.e., the trace spacing is 0.1 m and the maximum offset is 15 m. This second synthetic example was achieved with PSO parameter boundaries for the unsaturated first layer from 0.08 m/ns to 0.15 m/ns and for the saturated deeper layers from 0.09 m/ns to 0.04 m/ns, thickness range was kept in the range 0.2 m to 10 m for all layers. Thus we adapted search space boundaries, to ground water table expectation, for faster convergence and for more sensitivity for velocity changes between deeper layer in the water saturated zone, and we will proceed similarly with the field example.

The results of globally inverting the corresponding noise-free traveltime data set are presented in Fig. 5, where we visualize the median, the 25th to 75th, and the 5th to 95th percentile calculated from the final ensemble of model parameters. The input and the achieved medians of the results are indicated in the figures with circles and cross symbols, respectively. Comparing the input model parameters to the median layer velocities and thicknesses from our PSO based inversion illustrates that the input model is accurately reconstructed (maximum discrepancies <5 %) including the velocity variations in the saturated zone (layers two to five). However, the 25th to 75th and the 5th to 95th percentile values indicate uncertainties in the underlying parameter distributions in the order of 10% and 20%, respectively. While the velocity of the first layer is well resolved, the estimated uncertainties for the velocities of layers two to four indicate reduced confidence in resolving this alternating sequence with velocity contrasts of 10 m/μs. For comparison, we also show the results of NMO based spectral velocity analysis including a transformation into interval velocity using Dix's equation (blue symbols in Fig. 5). Although this analysis provides an impression of subsurface velocity variations (which can be used to aid traveltime picking and finding reasonable parameter constraints for our global inversion), the sharp velocity contrast between layers 1 and 2 causes an overestimation of the parameters of layer 2 in the order of 30%, which clearly illustrates the limitation of NMO based velocity analyses.

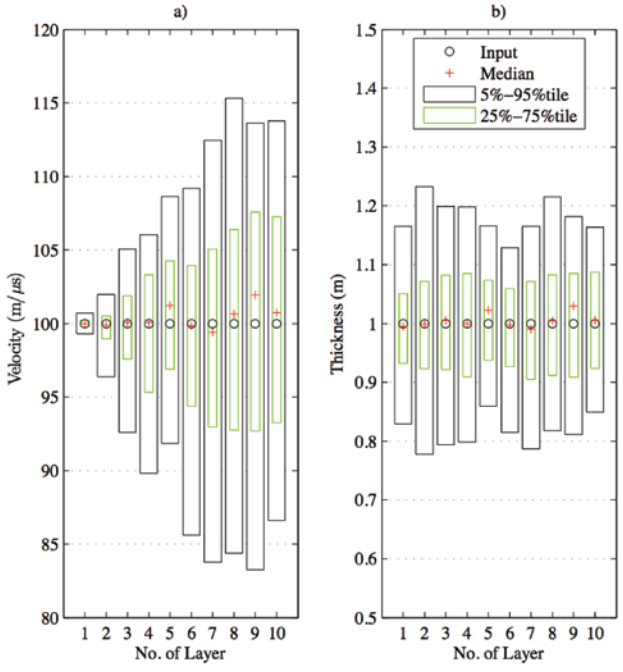

FIGURE 3

Results of globally inverting a synthetic reflection traveltime data set (example 1) including a comparison to the input model parameters. For (a) layer velocities and (b) layer thicknesses, the median, the 25th to 75th, and the 5th to 95th percentile calculated from the ensemble of models are shown. Layer number increases with increasing depth; i.e., number one represents the uppermost layer.

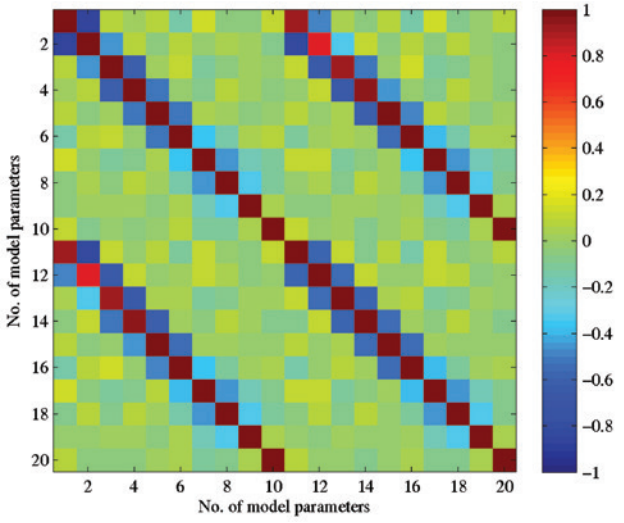

FIGURE 4

Model parameter correlation matrix calculated from the final ensemble of accepted models. Model parameters 1–10 correspond to the thicknesses of layers 1–10 while parameters 11–20 represent the corresponding layer velocities.

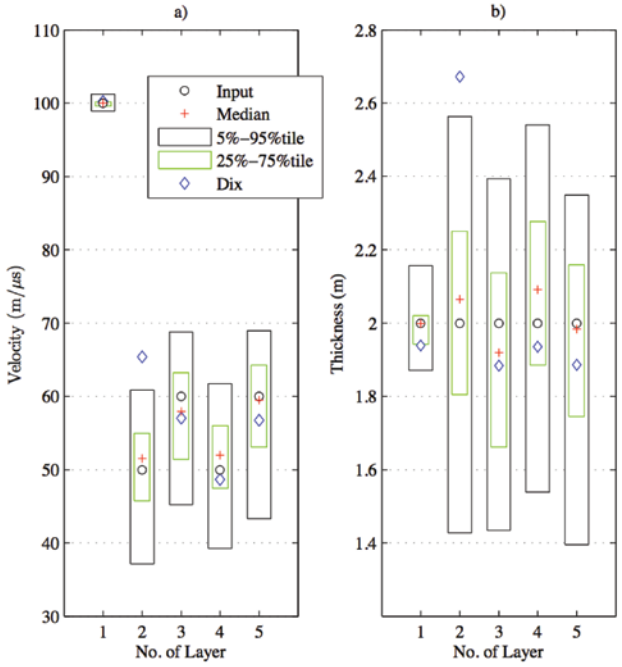

FIGURE 5
Results of globally inverting a synthetic reflection traveltime data set (example 2) including a comparison to the input model parameters and the results of NMO based analysis relying on Dix's equation. For (a) layer velocities and (b) layer thicknesses, the median, the 25th to 75th, and the 5th to 95th percentile calculated from the ensemble of models are shown. Layer number increases with increasing depth; i.e., number one represents the uppermost layer.

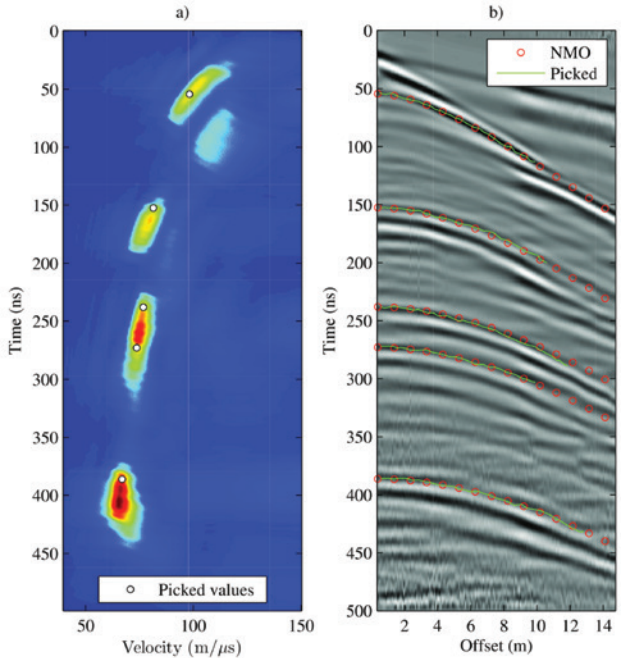

FIGURE 6
CMP field data example recorded at the Horstwalde test site, Germany. (a) NMO based velocity spectrum calculated from (b) the processed CMP data gather. In (a), yellow to red colours indicate maximum coherency values. In (b), the hyperbolic NMO events calculated using equation 1 and the picked values from (a) are indicated by red symbols while the green lines represent the traveltimes picked in the raw data section (not shown) which are used as input for our global inversion scheme.

In conclusion, the discussed and further synthetic examples (not shown here) demonstrate that our PSO based global inversion is a feasible tool to reconstruct 1D velocity models from typical CMP traveltime data even in the presence of sharp velocity contrasts. Furthermore, our approach provides reliable estimates of uncertainty, which, for example, show the challenge in resolving minor velocity variations underneath a shallow groundwater table using surface-based CMP data.

FIELD EXAMPLE

To demonstrate the applicability of our global inversion approach to field data, we use it to invert reflection traveltimes manually picked from a CMP data set recorded at a well constrained test site in Horstwalde, Germany. This site has been installed by the University of Potsdam and the German Federal Institute for Materials Research and Testing (BAM). As known from a variety of available borehole, direct-push, and geophysical data, the shallow geology is characterized by layered sequences of sand and gravel dominated glaciofluvial deposits showing only minor inclusions of clay, lignite, and organic material (Linder *et al*. 2010; Schmelzbach *et al*. 2011; Tronicke *et al*. 2012). Here, we focus on a single GPR CMP data set recorded close to borehole B1/09, where different borehole and direct-push logs are available (Tronicke *et al*. 2012). The data were recorded using 100 MHz antennae, a sampling interval of 0.1 ns, minimum and maximum source-receiver offsets of 0.4 m and 14.7 m, respectively, and stepwise offset increments of 0.1 m.

In Fig. 6, we present the CMP data section after amplitude scaling and bandpass filtering as well as the result of NMO based spectral velocity analysis calculated using the un-normalized cross-correlation as coherency measure. Five reflection events can be clearly identified by their hyperbolic moveout in the data section (Fig. 6b) and by the corresponding maximum values in the velocity spectrum (Fig. 6a). Inverting the picked values from the velocity spectrum using Dix's equation provides a first impression of subsurface velocity variations (blue symbols in Fig. 7). From this analysis, we learn that the first reflection characterizes the transition from unsaturated to water saturated sediments while the deeper reflections are associated with sedimentary structures in the saturated zone. While the unsaturated sediments up to a depth of ~3 m are characterized by velocities of ~100 m/μs, the results of NMO based analysis indicate velocities of ~60 m/μs for the saturated sediments up to a depth of ~12 m. Guided by the results of NMO based analysis we have manually picked the arrival times of the identified reflection events (Fig. 6b) in the raw data section (not shown). Furthermore, we

have used the NMO based velocity model to constrain the model space in our global inversion approach to reasonable values of the individual model parameter.

In Fig. 7, we illustrate the results of globally inverting the reflection traveltime data set. We show the median, the 25th to 75th, and the 5th to 95th percentile calculated from the ensemble of model parameter distributions (interval velocity and thickness of layers number one to five where layer number one corresponds to the uppermost layer) and also compare these values to the result of NMO based analysis. Comparable to our second synthetic example, the velocity and the thickness of the first layer are well resolved and we observe only minor differences between the results of global inversion and NMO based analysis. The thickness of the first layer is also in excellent agreement with the depth of the groundwater table measured during our GPR measurements at a depth of 2.73 m with a water level meter in the borehole. Also similar to our synthetic example, we notice increased uncertainties in the saturated zone (layers 2 to 5) and some significant differences (up to ~30%) between the global inversion result and the NMO based analysis. Again, these discrepancies are associated with the assumptions inherent in NMO based approaches; i.e., small offset-to-depth ratios and small velocity gradients across layer boundaries. Uncertainties of PSO are widened in contrast to the shown synthetic examples, which indicate the quality of the picked traveltimes in terms of noise, sampling precision and offset errors.

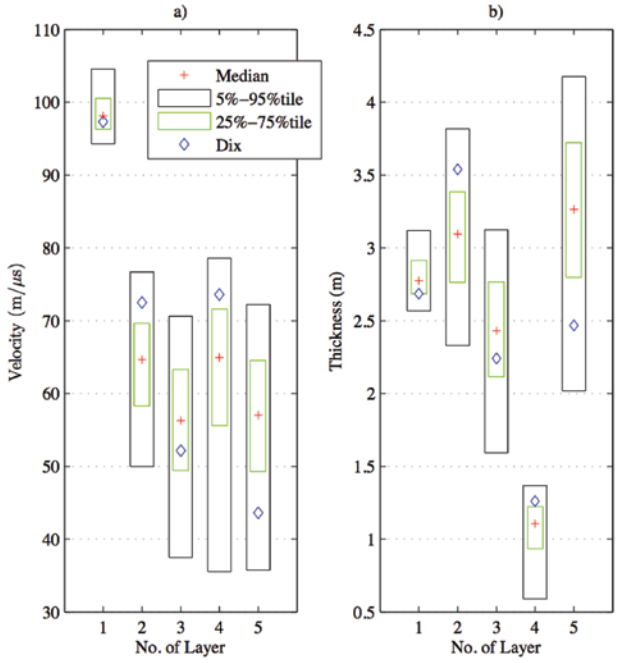

FIGURE 7

Results of globally inverting reflection traveltimes from the field data set including a comparison to the results of NMO based analysis relying on Dix's equation. For (a) layer velocities and (b) layer thicknesses the median, the 25th to 75th, and the 5th to 95th percentile calculated from the ensemble of models are shown. Layer number increases with increasing depth; i.e., number one represents the uppermost layer.

To further check the consistency of our derived velocity model including the derived estimates of uncertainty (Fig. 8a) with independent data, we compare it to two selected direct-push and borehole logs (Fig. 8b and 8c). The shown friction ratio log was measured using a standard cone-penetration test tool and is indicative for different soil types (Lunne *et al.* 1997). The log of natural gamma-ray (GR) activity was recorded with a constant logging speed using a standard borehole tool measuring activity in counts per second (cps). For each of the layers identified by our global traveltime inversion procedure, we have calculated the median and the 25th to 75th percentile values to characterize the central tendency and the variability of the two logging parameters within individual layers. In doing so, we basically upscale the core and logging data to the spatial scale of the structures imaged by our CMP data set. When comparing the parameter-depth models in Fig. 8, we see that the imaged velocity variations and depths of the interfaces, respectively, largely correspond to compositional changes indicated by the logging data. For example, for the

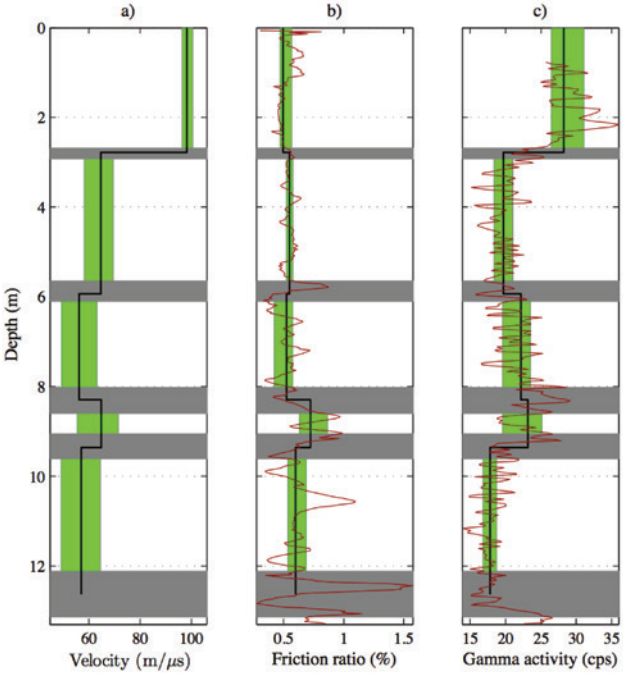

FIGURE 8

Comparison of global inversion results of the field data example to selected logs available at the CMP location at the test site. (a) CMP derived layer velocities as a function of depth, (b) friction ratio as function of depth as calculated from CPT logging data, and (c) natural gamma activity as derived from borehole GR logging data. In (a) to (c), grey boxes indicate depth uncertainties as estimated by the 25th to 75th percentile values from the global inversion result (Fig. 7). In (a), the green boxes indicate velocity uncertainties as estimated by the 25th to 75th percentile values from the global inversion result (Fig. 7), while in (b) and (c) the green boxes characterize the variability (25th to 75th percentile) of friction ratio and gamma activity, respectively, calculated from the logging data in the depth intervals defined by the median model in (a).

GR data (Fig. 8c) in the saturated zone (below depths of ~3 m) we notice increasing GR median and 25th to 75th percentile values with depth (layers 2 to 4) while the lowermost layer (layer 5) is characterized by minimum median values and minimum variability. A similar observation can be made for the friction ratio log (Fig. 8b), and we conclude that the derived 1D GPR velocity model is largely consistent with independent logging data.

CONCLUSION

In GPR surveying, CMP surveys are routinely employed to determine 1D velocity models collected at selected locations across a field site. We have presented a global inversion approach based on PSO to analyse reflection traveltimes observed in such CMP data sets. As our approach employs an accurate forward modelling routine which accounts for refraction effects, our methodology avoids the inherent assumptions of NMO based velocity analysis and, thus, provides more accurate velocity estimates than these standard analysis tools. Furthermore, our inversion approach can be used to generate an ensemble of acceptable solutions. Analysing a representative ensemble allows us to analyse the interdependence between different model parameters. The observed correlations between layer thicknesses and velocities within individual layers as well as with neighbouring layers illustrate the fundamental limitations of deriving accurate velocity estimates from a single CMP gather. From the generated ensemble of solutions, we also calculate different statistical measures to characterize the central tendency as well as the variability of the individual model parameters. For our synthetic and field examples, we have used the median, the 25th to 75th, and the 5th to 95th percentile to characterize the underlying parameter distributions and to provide reliable estimates of uncertainty. We found that great changes of velocity, such as those associated with a shallow groundwater table, decrease our ability to accurately resolve the model parameters for deeper layers. Because our PSO based inversion approach is easy to implement, needs less parameter adjustments, and provides faster convergence compared with other more common global optimization approaches (e.g., simulated annealing methods), we believe that the presented methodology is a feasible and powerful tool to analyse GPR CMP data and allows practitioners and researchers to evaluate the uncertainties of CMP derived velocity models.

REFERENCES

Al-Chalabi M. 1973. Series approximation in velocity and traveltime computations. *Geophysical Prospecting* **21**, 783–795.

Al-Chalabi M. 1974. An analysis of stacking, RMS, average, and interval velocities over a horizontally layered ground. *Geophysical Prospecting* **22**, 458–475.

Alkhalifah T. 1997. Velocity analyses using nonhyperbolic moveout in transversely isotropic media. *Geophysics* **62**, 1839–1854.

Annan A.P. 2005. Ground-penetrating radar. In: *Near Surface Geophysics*, (ed. D.K. Butler), pp. 357–438. SEG.

Aster R.C., Borchers B. and Thurber C.H. 2013. *Parameter Estimation and Inverse Problems.* Academic Press.

Becht A., Appel E. and Dietrich P. 2006. Analysis of multi-offset GPR data: A case study in a coarse-grained gravel aquifer. *Near Surface Geophysics* **4**, 227–240.

Binley A., Winship P., Middleton R., Pokar M. and West J. 2001. High-resolution characterization of vadose zone dynamics using cross-borehole radar. *Water Resources Research* **37**, 2639–2652.

Booth A.D., Linford N.T., Clark R.A. and Murray T. 2008. Three-dimensional, multi-offset GPR imaging of archaeological targets. *Archaeological Prospection* **15**, 1–20.

Booth A.D, Clark R.A. and Murray T. 2010. Semblance response to a ground-penetrating radar wavelet and resulting errors in velocity analysis. *Near Surface Geophysics* **8**, 235–246.

Booth A.D., Clark R.A. and Murray T. 2011. Influences on the resolution of GPR velocity analyses and a Monte Carlo simulation for establishing velocity precision. *Near Surface Geophysics* **9**, 399–411.

Bradford J.H. and Harper J.T. 2005. Wave field migration as a tool for estimating spatially continuous radar velocity and water content in glaciers. *Geophysical Research Letters* **32**, L08502.

Bradford J.H. 2006. Applying reflection tomography in the postmigration domain to multifold ground-penetrating radar data. *Geophysics* **71**, K1–K8.

Bradford J.H., Nichols J., Mikesell D. and Harper J. 2009. Continuous multi-fold acquisition and analysis of ground-penetrating radar data for improved characterization of glacier structure and water content. *Annals of Glaciology* **50**, 1–9.

Cai J. and McMechan G.A. 1999. 2-D ray-based tomography for velocity, layer shape, and attenuation from GPR data. *Geophysics* **64**, 1579–1593.

Cassiani G., Strobbia C. and Gallotti L. 2004. Vertical radar profiles for the characterization of deep vadose zones. *Vadose Zone Journal* **3**, 1093–1105.

Cassidy N. 2009. Ground penetrating radar data processing, modeling and analysis. In: *Ground penetrating radar: theory and applications*, (ed. H. Jol), pp. 141–172. Elsevier.

Clerk M. and Kennedy J. 2002. The particle swarm-explosion, stability, and convergence in a multidimensional complex space. *IEEE Transactions on Evolutionary Computation* **6**, 58–73.

Davis J.L. and Annan A.P. 1989. Ground-penetrating radar for high-resolution mapping of soil and rock stratigraphy. *Geophysical Prospecting* **37**, 531–551.

Dix C.H. 1955. Seismic velocities from surface measurements. *Geophysics* **20**, 68–86.

Eberhart R.C. and Shi Y. 2000. Comparing inertia weights and constriction factors in particle swarm optimization. *Proceedings of the IEEE Congress on Evolutionary Computation*, 84–88.

Fernández Martínez J.L., García Gonzalo E., Fernández Álvarez J.P., Kuzma H.A. and Menéndez Pérez C.O. 2010. PSO: A powerful algorithm to solve geophysical inverse problems-Application to a 1D-DC resistivity case. *Journal of Applied Geophysics* **71**, 13–25.

Fomel S. 1997. A variational formulation of the fast marching eikonal solver. *Stanford Exploration Project* **95**, 127–147.

Greaves R.J., Lesmes D. P., Lee J.M. and Toksoz M.N. 1996. Velocity variations and water content estimated from multi-offset, ground-penetrating radar. *Geophysics* **61**, 683–695.

Hajnal Z. and Sereda I.T. 1981. Maximum uncertainty of interval velocity estimates. *Geophysics* **46**, 1543–1547.

Hamann G., Tronicke J., Steelman C. and Endres A. 2013. Spectral velocity analysis for determination of ground wave velocities and their uncertainties in multi-offset GPR data. *Near Surface Geophysics* **11**, 167–176.

Harper J.T. and Bradford J.H. 2003. Snow stratigraphy over a uniform depositional surface: spatial variability and measurement tools. *Cold Regions Science and Technology* **37**, 289–298.

Huisman J.A., Hubbard, S.S., Redman, J.D. and Annan, A.P. 2003. Measuring soil water content with ground penetrating radar: a review. *Vadose Zone Journal* **2**, 476–491.

Jacob R.W. and Hermance J.F. 2004 Assessing the precision of GPR velocity and vertical two-way travel time estimates. *Journal of Environmental and Engineering Geophysics* **9**, 143–153.

Jol H.M. 2008. *Ground Penetrating Radar Theory and Applications*. Elsevier Science.

Kennedy J. and Eberhart R.C. 1995. Particle swarm optimization. In: *Proceedings of the IEEE International Joint Conference on Neural Networks*, Vol. **4**, pp. 1942–1948, IEEE.

Leparoux D., Gibert D. and Cote P. 2001. Adaptation of prestack migration to multi-offset ground-penetrating radar (GPR) data. *Geophysical Prospecting* **49**, 374–386.

Levin F.K. 1971. Apparent velocity from dipping interface reflections. *Geophysics* **36**, 510–516.

Linder S., Paasche H., Tronicke J., Niederleithinger E. and Vienken T. 2010. Zonal cooperative inversion of crosshole P-wave, S-wave, and georadar traveltime data sets. *Journal of Applied Geophysics* **72**, 254–262.

Lunne T., Robertson P.K. and Powell, J.J.M. 1997. *Cone Penetration Testing in Practice*. Blackie Academic and Professional.

Menke W. 1989. *Geophysical Data Analysis: Discrete Inverse Theory*. Elsevier, 45.

Monteiro Santos F.A. 2010. Inversion of self-potential of idealized bodies' anomalies using particle swarm optimization. *Computers & Geosciences* **36**, 1185–1190.

Moore J.C., Pälli A., Ludwig F., Blatter H., Jania J., Gadek B., Glowacki P. *et al*. 1999. High-resolution hydrothermal structure of Hansbreen, Spitsbergen, mapped by ground-penetrating radar. *Journal of Glaciology* **45**, 524–532.

Pipan M., Baradello L., Forte E., Prizzon A. and Finetti I. 1999. 2D and 3D processing and interpretation of multi-fold ground penetrating radar data: a case history from an archaeological site. *Journal of Applied Geophysics* **41**, 271–292.

Poli R. 2008. Analysis of the publications on the applications of particle swarm optimization. *Journal of Artificial Evolution and Applications* **1**, 1–10.

Porsani J.L. and Sauck W.A. 2007. Ground-penetrating radar profiles over multiple steel tanks: Artifact removal through effective data processing. *Geophysics* **72**, J77–J83.

Schmelzbach C., Tronicke J. and Dietrich P. 2011. Three-dimensional hydrostratigraphic models from ground-penetrating radar and direct-push data. *Journal of Hydrology* **398**, 235–245.

Sen M.K. and Stoffa P.L. 1995. *Global Optimization Methods in Geophysical*. Elsevier Science B.V.

Sethian J.A. 1996. A fast marching level set method for monotonically advancing fronts. In: *Proceedings of the National Academy of Sciences of USA*, Vol. 93, pp. 1591–1595.

Sethian J.A. and Popovici A.M. 1999. 3-D traveltime computation using the fast marching method. *Geophysics* **64**, 516–523.

Shaw R. and Srivastava S. 2007. Particle swarm optimization: A new tool to invert geophysical data. *Geophysics* **72**, F75–F83.

Steelman C.M. and Endres A.L. 2012. Assessing vertical soil moisture dynamics using multi-frequency GPR common-midpoint soundings. *Journal of Hydrology* **436-437**, 51–-66.

Taner M.T. and Koehler F. 1969. Velocity spectra-digital computer derivation and applications of velocity functions. *Geophysics* **34**, 859–881.

Tarantola A. 2005. *Inverse Problem Theory and Methods for Model Parameter Estimation*. Society for Industrial and Applied Mathematics.

Tillard S. and Dubois J.C. 1995. Analysis of GPR data: wave propagation velocity determination. *Journal of Applied Geophysics* **33**, 77–91.

Tronicke J., Dietrich P., Wahlig U. and Appel E. 2002. Integrating GPR and crosshole radar tomography: A validation experiment in braided stream deposits. *Geophysics* **67**, 1495–1504.

Tronicke J., Holliger K., Barrash W. and Knoll M.D. 2004. Multivariate analysis of crosshole georadar velocity and attenuation tomograms for aquifer zonation. *Water Resources Research* **40**, WO1519.

Tronicke J. and Knoll M.D. 2005. Vertical radar profiling: Influence of survey geometry on first arrival traveltimes and amplitudes. *Journal of Applied Geophysics* **57**, 179–191.

Tronicke J., Paasche H. and Böniger U. 2012. Crosshole traveltime tomography using particle swarm optimization: a near-surface field example. *Geophysics* **77**, R19–R32.

Van den Bergh F. 2002. *An analysis of particle swarm optimizers*. Ph.D Thesis, University of Pretoria.

Van Overmeeren R.A., Sariowan S.V. and Gehrels J.G. 1997. Ground penetrating radar for determining volumetric soil water content; results of comparative measurements at two test sites. *Journal of Hydrology* **197**, 316–338.

Wilken D. and Rabbel W. 2012. On the application of Particle Swarm Optimization strategies on Scholte-wave inversion. *Geophysical Journal International* **190**, 580–594.

Yilmaz Ö. 2001. *Seismic Data Analysis: Processing, Inversion, and Interpretation of Seismic Data*. Tulsa: Society of Exploration Geophysicists.

Zelt C.A. and Smith R.B. 1992. Seismic traveltime inversion for 2-D crustal velocity structure. *Geophysical Journal International* **108**, 16–34.